Medicinal Chemistry Research (2019) 28:1–12
https://doi.org/10.1007/s00044-018-2257-y

MEDICINAL CHEMISTRY RESEARCH

ORIGINAL RESEARCH

Dioscin-6′-O-acetate impairs migration of lung cancer cells through attenuations of MMP-2 and MMP-9 via NF-κB suppression

Xuejiao Li[1] · Jiachen Sun[2] · Xia Li[1] · Yujie Dai[3] · Chengcheng Zhao[1] · Shuli Man[3] · Ying Wang[4] · Wenyuan Gao[1,3,4]

Received: 5 September 2018 / Accepted: 30 October 2018 / Published online: 14 November 2018

Abstract

More than 90% of the cancer-associated mortality is attributed to its metastasis. Numerous studies demonstrated that natural steroidal saponins from plants had the capacity to inhibit lung cancer metastasis. Dioscin-6'-O-acetate (DA) was a novel steroidal saponin first obtained from the rhizomes of *Dioscorea althaeoides* R. Knuth. Our previous study indicated that it suppressed lung cancer cell proliferation via inducing cell-cycle arrest and enhancing caspase-dependent apoptosis. Until now, there were still no reports on its anti-migration activity. In the present study, we further verified the anti-proliferation and apoptosis-inducing effects and investigated the anti-migration effects of DA on human NSCLC (NCI-H460, NCI-H1299, NCI-H520) and SCLC (NCI-H446) cells for the first time. To clarify the possible mechanisms, western blot and/or RT-PCR analysis were used. The results revealed that DA treatment increased the levels of caspase 3, 8, 9, and Bax and markedly decreased the expression of bcl-2, PCNA, MMP-2, MMP-9, and NF-κB. Docking study indicated that DA presented strong affinity with the key metastasis-related proteins, such as MMP-2, MMP-9, and NF-κB. We proposed that DA might suppress lung cancer proliferation by downregulating PCNA, induce lung cancer apoptosis via activation of caspase-dependent apoptosis pathways, and inhibit lung cancer migration possibly by targeting MMP-2/9 through NF-κB signaling suppression. The findings would provide the foundation for the clinical use of DA in future.

Keywords Dioscin-6'-O-acetate · Lung cancer · Migration · MMP-2 · MMP-9 · NF-κB

Introduction

Lung cancer is a predominant type of malignancy with the highest morbidity and mortality worldwide (Wang et al. 2018; Siegel et al. 2017; El Gaafary et al. 2017; Siegel et al. 2016). Non-small cell lung cancer (NSCLC) accounts for about 85% of lung cancers, with a 5-year survival rate of <15%, while small cell lung cancer (SCLC), another type of lung cancer with a 5-year survival rate of 6%, is the most aggressive lung cancer form (Liu et al. 2017). More than 90% of the cancer-associated mortality can be attributed to its metastasis (Li et al. 2018a). A total of 80–90% of NSCLC patients have distant metastasis upon diagnosis or during treatment (Wang et al. 2018). Owing to these obstacles, it is difficult to treat lung cancers effectively. Thus novel effective drugs either targeting or preventing its ongoing metastasis are urgently needed for combating this malignancy.

Metastasis is a complex process that is regulated by multiple genes. The degradation of the extracellular matrix (ECM) via protease is a crucial step during tumor invasion or migration (Wang et al. 2018). As a family of enzymes

These authors contributed equally: Xuejiao L, Jiachen Sun.

Electronic supplementary material The online version of this article (https://doi.org/10.1007/s00044-018-2257-y) contains supplementary material, which is available to authorized users.

✉ Shuli Man
msl@tust.edu.cn

✉ Wenyuan Gao
biochemgao@163.com

[1] Tianjin Key Laboratory for Modern Drug Delivery & High-Efficiency, School of Pharmaceutical Science and Technology, Tianjin University, 300072 Tianjin, China

[2] School of Biotechnology and Food Science, Tianjin University of Commerce, 300134 Tianjin, China

[3] Tianjin Key Laboratory of Industry Microbiology, College of Biotechnology, Tianjin University of Science & Technology, 300457 Tianjin, China

[4] Tianjin Key Laboratory of Chemistry and Analysis of Chinese Materia Medica, Tianjin University of Traditional Chinese Medicine, 300193 Tianjin, China

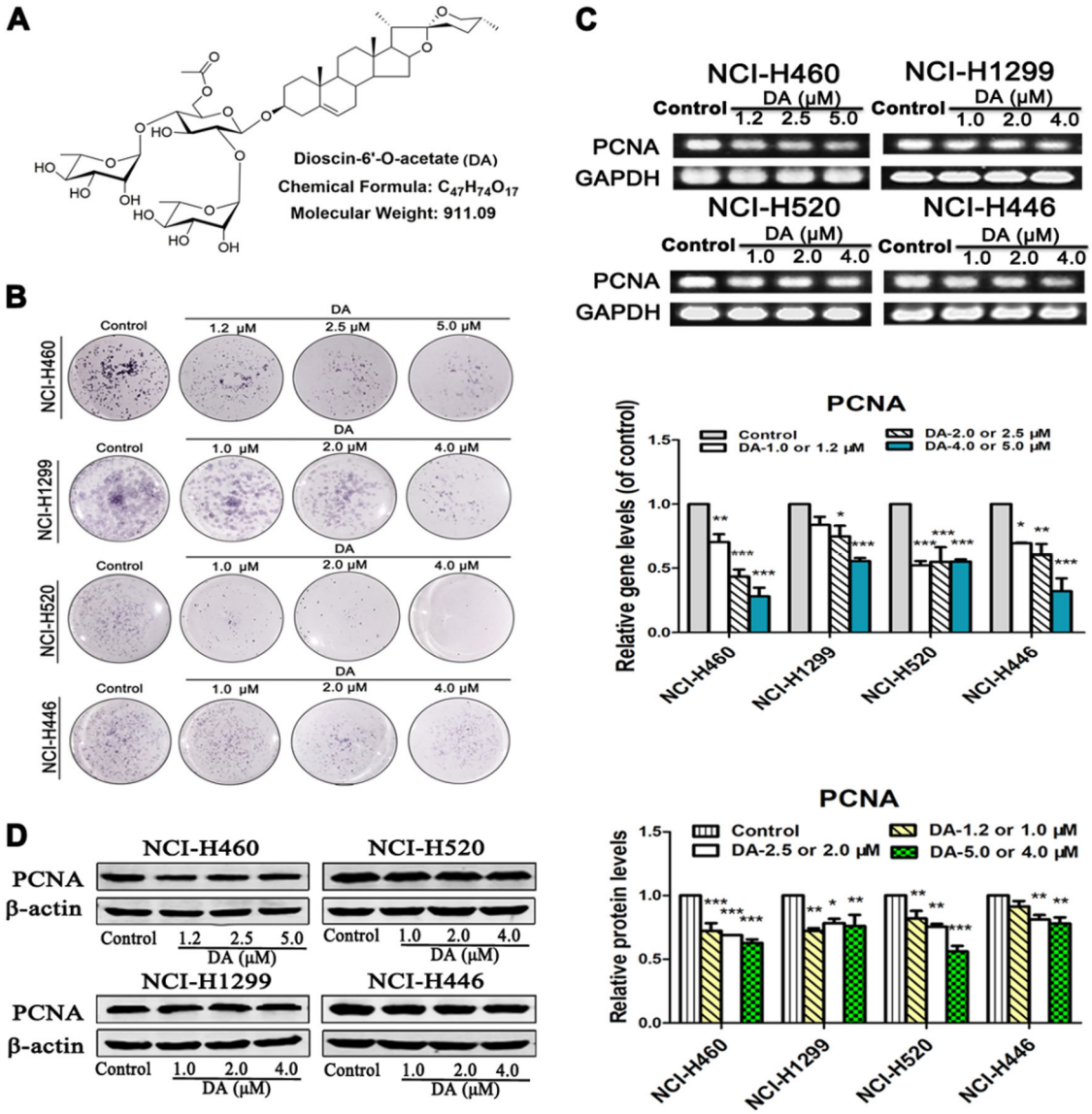

Fig. 1 The anti-proliferative effect of DA on four lung cancer cells. **a** Chemical structure of dioscin-6'-O-acetate (DA). **b** The colony-formation assay of DA. **c**, **d** Effects of DA (0–5.0 μM) on the mRNA and protein levels of PCNA. Data are presented as mean ± S.D. of at least three independent experiments (*$P < 0.05$, **$P < 0.01$, ***$P < 0.001$ vs control group)

degrading the ECM, the matrix metalloproteinases (MMPs), particularly MMP-2 and MMP-9, are strongly implicated in the invasion and metastasis of malignant tumors and a poor prognosis in cancer patients (Kim et al. 2017). MMP-2 and MMP-9, which are overexpressed during tumor metastasis, have a unique capability to use mainly collagen IV as substrate and digest the basement membrane to promote the migration of transdifferentiated cells into the submesothelial area in cancer metastasis (Lupinacci et al. 2018; Asghar et al. 2018). Nuclear factor (NF)-κB signaling pathway is involved in cell metastasis and migration by modulating the expression of downstream targets, including MMPs (Garg et al. 2010). Hence, targeting NF-κB and MMPs could prevent tumor metastasis and consequently reduce mortality.

Previous studies shown that natural steroidal saponins derived from plants had the capacity to inhibit lung cancer metastasis through the downregulation of MMP-2 and MMP-9 (Jung et al. 2016; Lim et al. 2017; Si et al. 2016). The extraction of *Dioscorea nipponica* Makino (Dioscoreaceae) inhibits migration and invasion of human oral cancer HSC-3 cells by transcriptional inhibition of MMP-2 through modulation of c-AMP-responsive element-binding protein and activator protein 1 activity (Chien et al. 2012). Dioscin-6'-O-acetate (DA; Fig. 1a), a novel steroidal saponin, was first isolated from the rhizomes of *Dioscorea althaeoides* R. Knuth (Dioscoreaceae) (Li et al. 2016). Its deacetylation analogue, dioscin existing in most of Dioscorea plants, induced human lung cancer cell apoptosis and

autophagy through suppression of phosphoinositide-3 kinase (PI3K)/AKT/mammalian target of rapamycin (mTOR), activation of mitogen-activated protein kinase (MAPK) signaling pathways and activation of mitochondrial signal pathway (Wei et al. 2013; Hsieh et al. 2013). Furthermore, dioscin remarkably impaired lung cancer migration via inhibiting transforming growth factor-beta 1 (TGF-β1)-regulated activation of MMP-2/9 (Lim et al. 2017), although our previous study indicated that DA suppressed lung cancer cell proliferation via inducing cell-cycle arrest and enhancing caspase-dependent apoptosis, at least partly, through reactive oxygen species-mediated PI3K/AKT, MAPK, and NF-κB signaling pathways (Li et al. 2019). The anti-migration activities and precise molecular mechanisms of DA have not been understood. The aim of the present study was to further elucidate the anti-proliferation, apoptosis-inducing and anti-migration effects, and possible mechanisms of DA on human NSCLC (NCI-H460, NCI-H1299, NCI-H520) and SCLC (NCI-H446) cells.

Materials and methods

Reagents

DA was isolated by our laboratory (Li et al. 2016) with the purity a 98% (for ^{1}H and ^{13}C nuclear magnetic resonance spectra, see Figs. S1 and S2; for HPLC chromatogram, see Fig. S3). Hoechst 33258, acridine orange (AO), and ethidium bromide (EB) fluorescent dyes were all obtained from Solarbio Science and Technology Co. (Beijing, China). The other reagents were of analytical purity.

Cell lines and culture

Human lung large cell carcinoma NCI-H460 (H460), human lung adenocarcinoma NCI-H1299 (H1299), human lung squamous cell carcinoma NCI-H520 (H520), and SCLC NCI-H446 (H446) were acquired from Shanghai Institutes of Biological Sciences, Chinese Academy of Sciences (Shanghai, China). The human lung cancer cells were cultured in RPMI-1640 medium supplemented with 10% fetal bovine serum (PAN-Biotech GmbH, German) and 1% penicillin–streptomycin (100 units/mL, 100 mg/mL) at 37 °C in a humidified incubator containing 5% CO_2.

Colony-formation assay

Lung cancer cells (800/well) were incubated for 7 days in a 6-well plate. Different concentrations of DA (0–5.0 μM) were added. The cells were incubated with DA for another 5 days. Then 3-[4,5-dimethylthiazol-2-yl]-2,5 diphenyl tetrazolium bromide (MTT) solution (0.5 mg/mL) was added and incubated for 4 h. Finally, the status of colony formation was recorded by a camera.

AO/EB and Hoechst 33258 staining

After treatment with DA (0–5.0 μM) for 24 h, the cells were washed with phosphate-buffered saline (PBS) thrice and then fixed in 100% ice-cold methanol for 5 min. After washing in PBS thrice, the nuclei were stained with AO/EB staining solution (100 mg/mL AO and 100 mg/mL EB in PBS) or Hoechst 33258 (1 μg/mL) for 15 min and observed by fluorescence microscopy with filters for ultraviolet (NikonN-STORM). Quantification of apoptotic cells in AO/EB staining assay was performed using the ImageJ software.

Wound-healing scratch assay

The cancer cells were cultured in 6-well plates for 24 h at 37 °C. Wounds were created in the cell monolayer and washed with PBS to remove cell debris, thereby treated with different concentrations of DA for 24 h or treated with DA (5.0 or 4.0 μM) for different treatment times. After that, the dead cells were washed away with PBS thrice, and the images were taken by the fluorescence microscope (NikonN-STORM).

Reverse transcription polymerase chain reaction (RT-PCR)

Lung cancer cells were seeded in 6-well plates (2.5×10^5/well) and incubated with 0–5.0 μM of DA for 24 h. Then cells were extracted with TRIzol (Life Technologies Inc.) according to the manufacturer's instruction. The quality of RNA was assessed by the absorbance of the samples at 260 and 280 nm. cDNA synthesis (Table S1) was performed using RevertAidTM M-MuLV RT (Fermentas, Hanover, MD, USA) according to the supplier's protocol. Resulting RT products were stored at −80 ℃ until analysis. A series of cDNA was amplified in PCR reactions consisting of 1× Taq polymerase buffer with 1.5 mM of $MgCl_2$ (Promega, Madison, WI), 200 mM of each dNTP, 10 pmol of each primer pair, and 1 U of Taq DNA polymerase (Promega). PCR products were analyzed by electrophoresis on 3.0% agarose gel and visualized after ethidium bromide staining.

Western blot analyses

The harvested protein was diluted by 4× SB loading buffer (Solarbio Science and Technology Co., China) and boiled for 5 min before loading onto sodium dodecyl sulfate-polyacrylamide gel electrophoresis (SDS-PAGE) gels. The

protein samples were separated by SDS-PAGE and transferred to a polyvinylidene difluoride (PVDF) membrane. After blockage of non-specific binding sites, the membrane was incubated overnight at 4 °C with various primary antibodies. The primary antibodies were NF-κB p65, proliferating cell nuclear antigen (PCNA; Santa Cruz Biotechnology, USA), MMP-2, and MMP-9 (Boster Biological Technology Co. Ltd., China). A β-actin antibody (Santa Cruz Biotechnology, USA) was used as a control for equal loading. After washing with PBST buffer solution thrice, PVDF membrane was incubated with IRDye® 680LT goat anti-mouse or goat anti-rabbit IgG secondary antibody (LI-COR Biotechnology, USA) for 2 h. Then the expression of protein was detected by Odyssey infrared imaging system (LI-COR Biotechnology, USA). Densitometric analysis of protein expression was performed using the ImageJ software and the values were normalized to those of β-actin.

Molecular docking

Docking simulations were carried out by using AutoDock Vina program (version 1.1.2).(Trott and Olson 2010) Three-dimensional structures of DA were downloaded from PubChem Compound (http://pubchem.ncbi.nlm.nih.gov). The structure of NF-κB (PDB code: 4Q3J), MMP-9 (PDB code: 1GKC), and MMP-2 (PDB code: 3AYU) were obtained from the protein data bank (http://www.rcsb.org/pdb). Receptors were prepared by removing water molecules and impurity ions, extraction of co-crystallized ligand, and adding polar hydrogen atoms. Docking calculations were performed based on the Lamarckian genetic algorithm. The predicted binding energy (kcal/mol) was calculated. The most reasonable complex structures were identified according to binding energy.

Statistical analysis

Data was expressed as mean ± S.D. of at least three independent experiments. Significant differences among groups in this study were analyzed by one-way analysis of variance test and Dunnett's test. A value <0.05 was considered to be statistically significant. All statistical analyses were performed with SPSS the IBM SPSS Statistics 21.

Results

DA inhibited proliferation of lung cancer cells

The MTT results of previous study indicated that DA caused less growth arrest in the normal lung BEAS-2B cells than that in the four lung cancer cells (Li et al. 2018b). Based on the IC_{50} values, the concentrations of 1.2, 2.5, and 5.0 μM for NCI-H460 cells and 1.0, 2.0, and 4.0 μM for NCI-H1299, NCI-H520, and NCI-H446 cells were chosen in the following assays.

The long-term anti-proliferative effect of DA was tested by colony-formation assay. The results revealed that DA dose-dependently reduced the clonogenicity of four cancer cells (Fig. 1b). Moreover, the mRNA and protein levels of PCNA were both significantly downregulated by DA (Fig. 1c, d). Our results revealed that DA significantly inhibited proliferation of four lung cancer cells by downregulation of PCNA.

DA induced apoptosis of four lung cancer cells

The effects of DA on apoptosis of NCI-H460, NCI-H1299, and NCI-H520 human NSCLC cells and NCI-H446 human SCLC cells were detected by AO/EB and Hoechst 33258 staining assay. Hoechst 33258 staining revealed that the condensed chromatin of cell nuclei and the nuclear fragmentation were observed in DA-treated lung cancer cells (Fig. 2a). Consistently, in AO/EB staining assay (Fig. 2a), obvious orange-colored to red-colored fluorescence of the apoptotic cells was observed in DA-treated lung cancer cells. The quantification results of apoptotic cells in AO/EB assay revealed that DA induced observable apoptosis in four lung cancer cells (Fig. 2b). To evaluate the relevant mechanisms of DA-induced apoptosis, the levels of apoptosis-related mRNA were determined by RT-PCR. As shown in Fig. 3, treatment with DA for 24 h remarkably upregulated the mRNA levels of Bax, caspase-3/-9, and poly ADP-ribose polymerase (PARP) and prominently suppressed the expression of bcl-2 in four human lung cancer cells. In addition, the mRNA levels of caspase-8 in NCI-H460, NCI-H1299, and NCI-H520 cells were significantly increased, along with a slight upregulation in NCI-H446 cells. All the above results demonstrated that DA exerted anti-proliferation effects on human lung cancer cells by inducing apoptosis, at least partially, through activation of the caspase-dependent pathway.

DA suppressed the migration of lung cancer cells via attenuations of MMP-2 and MMP-9

Tumor invasion and metastasis are the hardest problems in tumor treatment, especially for lung cancers. As shown in Fig. 4a, b, the capacities of wound healing of human NCI-H460, NCI-H1299, NCI-H520, and NCI-H446 cells were significantly attenuated by DA in a dose-dependent manner. The wound-healing area (percentage of 0 h) of NCI-H460 cells in control group at 72 h only reached to 42.65%, while that of NCI-H1299 (at 36 h), NCI-H520 (at 36 h), and NCI-H446 (at 48 h) cells was dramatically increased to 92.03, 81.49, and 98.37%, respectively, indicating that the

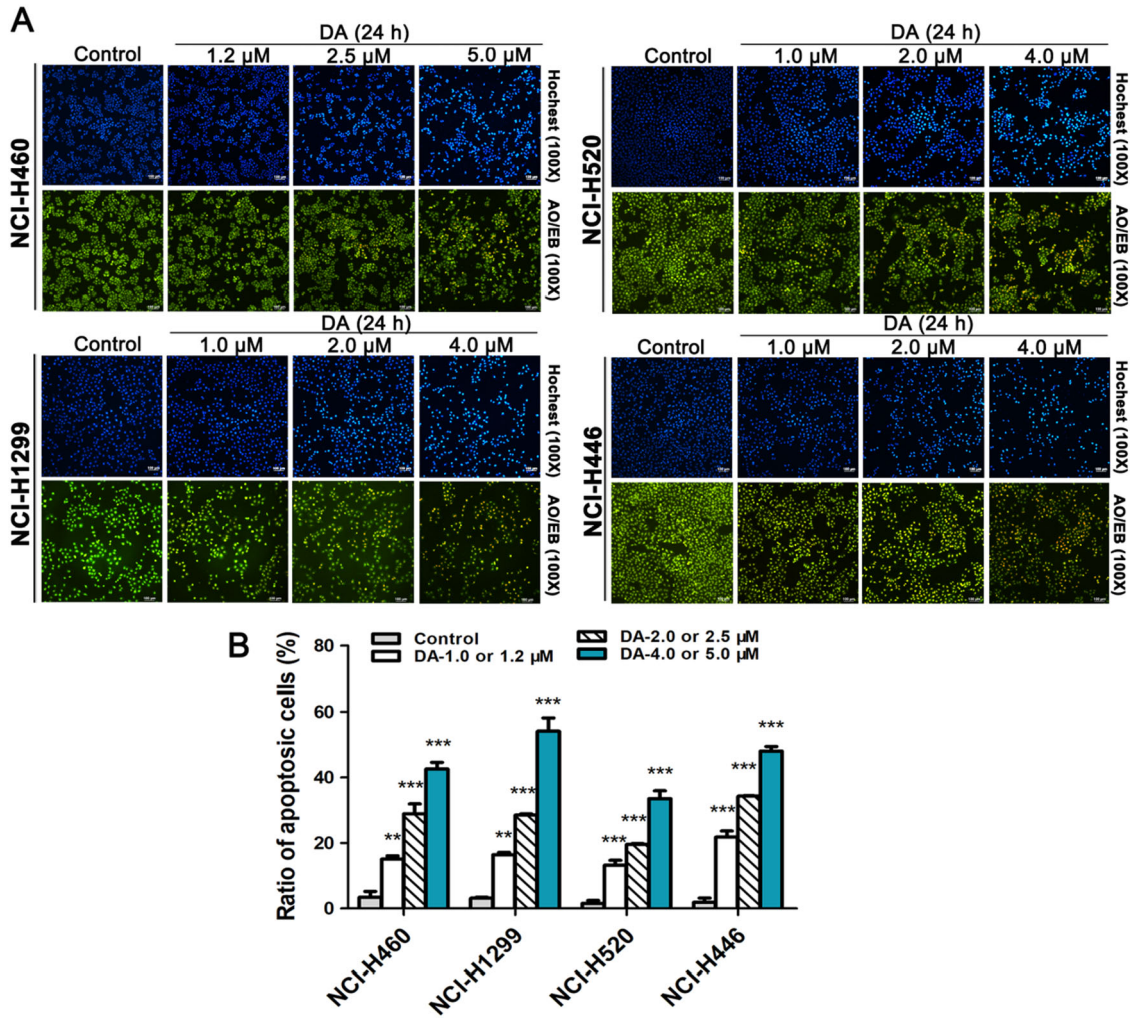

Fig. 2 The morphological changes of the cells treated by DA (0–5.0 μM) for 24 h. **a** Fluorescence images of lung cancer cells stained by Hoechst 33258 and AO/EB. For the AO/EB assay, the normal cells are green in color, early apoptosis yellow in color, late apoptosis orange in color, and necrosis red in color. **b** Quantification of apoptotic cells in AO/EB double-staining assay using the ImageJ software. Data are presented as mean ± S.D. of at least three independent experiments (**$P < 0.01$, ***$P < 0.001$ vs control group) (color figure online)

invasion ability of NCI-H1299, NCI-H520, and NCI-H446 was much stronger than that of NCI-H460. However, DA treatment could sharply weaken the migration of the three lung cancer cells, as well as the NCI-H460 cells. In addition, DA exerted significant inhibitive effect on the protein levels of MMP-2 and MMP-9 in a concentration-dependent manner (Fig. 4c). Moreover, the mRNA levels of NF-κB and protein expression of NF-κB p65 in the nucleus in NCI-H460, NCI-H1299, NCI-H520, and NCI-H446 lung cancer cells were all significantly downregulated by DA treatment (Fig. 5a, b).

Molecular docking

To investigate the interaction between DA and key metastasis-related proteins, molecular docking experiments were analyzed by AutoDock Vina program. The "blind docking" approach was used in order to find the binding site of DA in NF-κB p65/p50, MMP-9, and MMP-2. The blind docking studies revealed that main binding sites of DA (Fig. 6a1–c1). More details about DA-binding these sites are shown in Table 1. For NF-κB p65/p50 (PDB: 1IKN), there were three main binding sites. Site 1 showed an apparent high affinity for DA, in contrast to sites 2 and 3 (Fig. 6a2). The blind docking experiments revealed that DA preferentially bounded to the site 1 in MMP-9 (PDB: 1GKC; Fig. 6b). DA had three pose among the top-ranked poses binds to the site 1 in MMP-2 (PDB: 3AYU; Fig. 6c). On the basis of the above results, we proposed the site 1 as a potential binding site and aimed to reveal their molecular inhibitory mechanisms.

The binding mode of DA, with the best docking score and interaction in the binding site, is shown in Fig. 7. DA bounded to the active binding sites of NF-κB p65/p50,

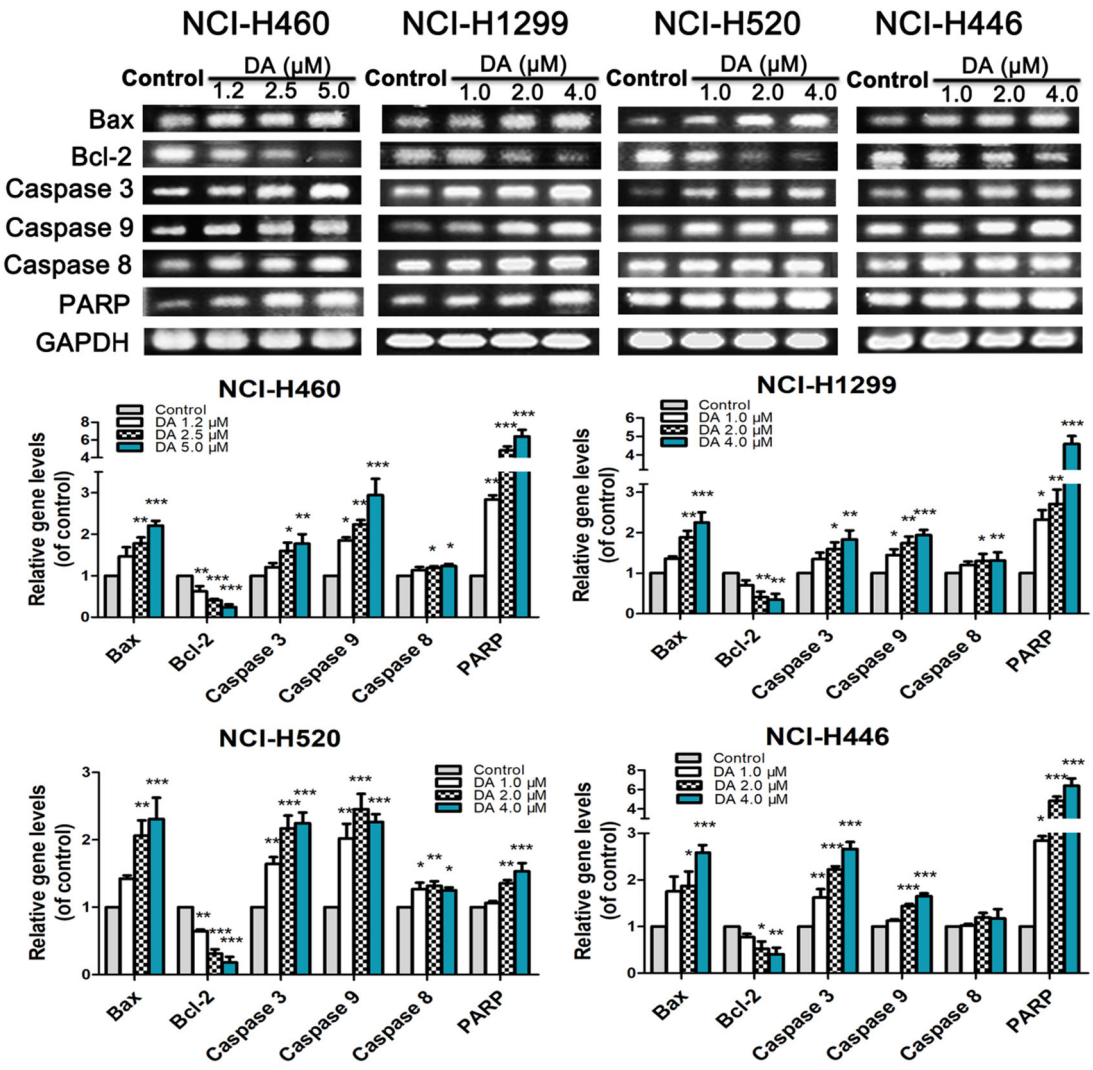

Fig. 3 Apoptosis-related mRNA in human lung cancer cells. The mRNA levels were normalized with GADPH levels. Data are presented as mean ± S.D. of at least three independent experiments (*$P < 0.05$, **$P < 0.01$, ***$P < 0.001$ vs control group)

MMP-9, and MMP-2 with the lowest binding energy of −8.4 kcal/mol, −8.2 kcal/mol, and −8.0 kcal/mol, respectively. The main interactions between DA and the active binding sites of NF-κB p65/p50, MMP-9, and MMP-2 were hydrophobic interactions and hydrogen bonds. Four hydrogen bonds were found between the hydroxyl groups at the sugar moiety of DA and the residues Asn200A, Glu264C, and Glu350C of NF-κB p65/p50. Meanwhile, the sapogenin part of DA was adjacent to two amino acid residues Tyr348C and Ile351C of NF-κB p65/p50 via hydrophobic interactions. Two hydrogen bonds of Glu111A and Ala191A with the hydroxyl groups in the glycoside of DA were largely responsible for the interaction between DA and MMP-9. Moreover, there was also hydrophobic contact between Tyr423A of MMP-9 and the sapogenin part of DA. Seven hydrogen bonds were found between the hydroxyl groups of DA and the residues Ala83A, His124A, Glu129A, and His130A of MMP-2. Simultaneously, there were also hydrophobic contacts between Phe4A and Pro8A of MMP-2 and the sapogenin part.

In order to validate the docking experiment that was used, we analyzed active sites between actual pose of the co-crystallized inhibitor and the docking ligand into their respective binding sites in NF-κB p65/p50, MMP-9, and MMP-2. Figure 8 showed the superimposition between the best docking result and the crystallographic geometry. In NF-κB p65/p50 (PDB ID: 1IKN), the site 1 was situated not far from the location previously identified as the active site (Huxford et al. 1998). The proximity of these two sites, as well as the high affinity of DA for this binding site, suggested that site 1 played an important role in the bioactivity of MMP-9 (PDB ID: 1GKC) (Rowsell et al. 2002). For MMP-2 (PDB ID: 3AYU), site 1 was rather narrow and deep, adjacent to the active site of co-crystallized inhibitor.

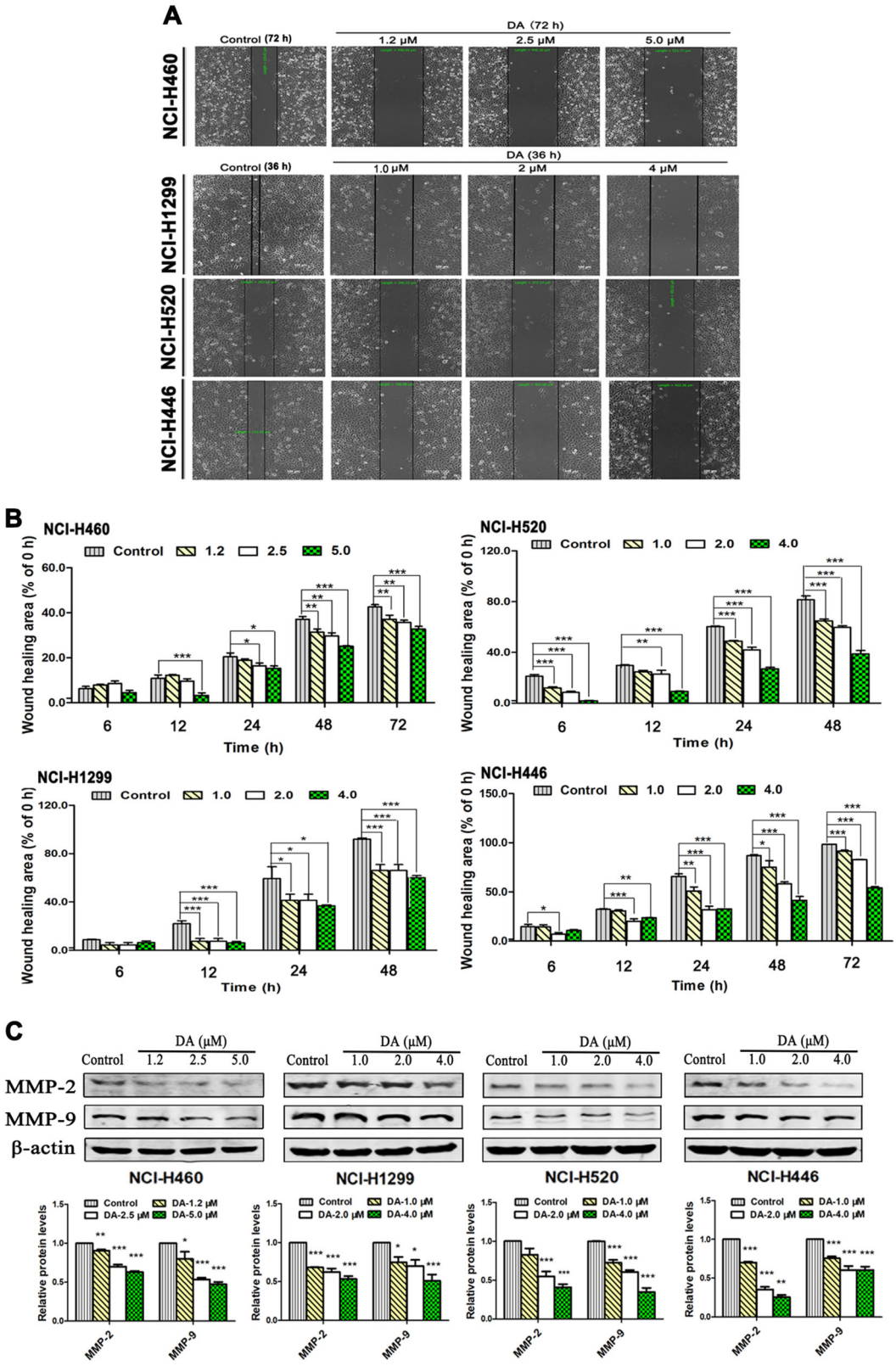

Fig. 4 DA inhibits the migration of four human lung cancer cells. **a** Representative wound-healing images of lung cancer cells treated by different dose of DA; **b** wound-healing area of lung cancer cells treated with DA (0–5.0 μM) for different times. **c** Effects of DA (0–5.0 μM) on the protein levels of MMP-2 and MMP-9. Protein levels were normalized with β-actin levels. Data are presented as mean ± S.D. of at least three independent experiments (*$P < 0.05$, **$P < 0.01$, ***$P < 0.001$ vs control group)

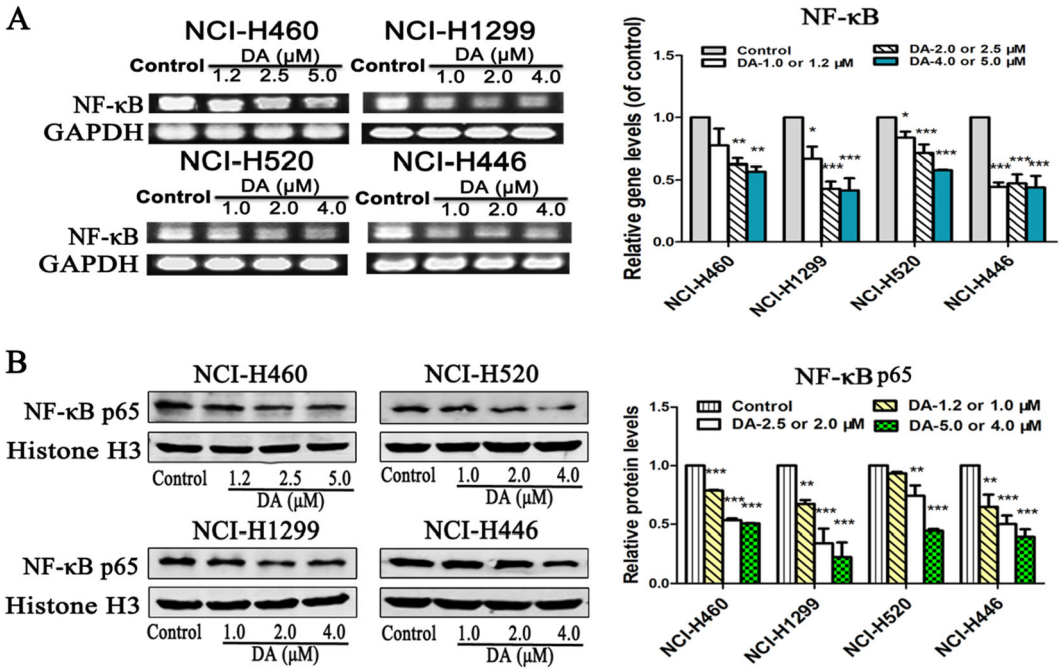

Fig. 5 Effects of DA on NF-κB signaling pathway in lung cancer cell lines. **a** mRNA levels were normalized with GADPH levels. **b** Protein levels of NF-κB p65 in the nucleus of lung cancer cells were normalized with histone H3 levels. Data are presented as mean ± S.D. of at least three independent experiments (*$P < 0.05$, **$P < 0.01$, ***$P < 0.001$ vs control group)

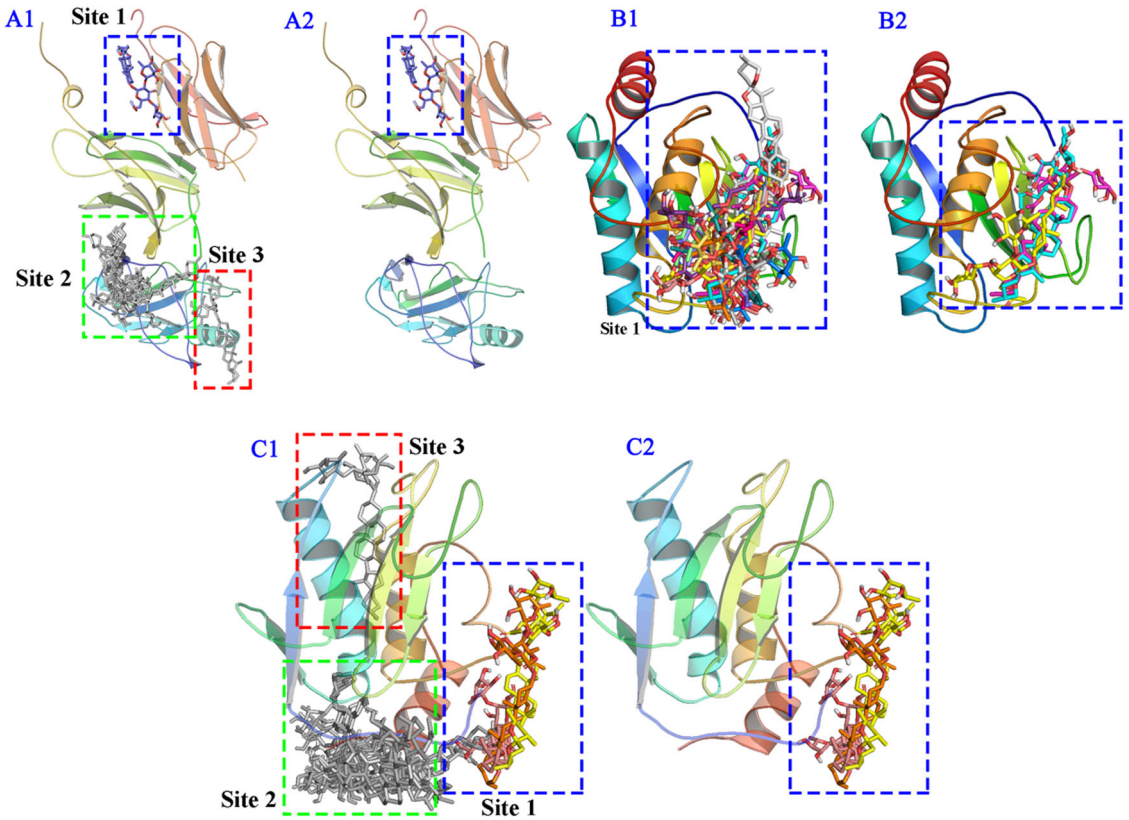

Fig. 6 Docking poses of DA binding to **a** NF-κB p65/p50 (PDB: 1IKN), **b** MMP-9 (PDB: 1GKC), and **c** MMP-2 (PDB: 3AYU). **a**1, **b**1, **c**1 Top blind docking poses were listed. Poses at the proposed active sites are shown in different colors with the rest in gray. **a**2, **b**2, **c**2 Top-scoring DA-focused docking poses at the proposed active sites (color figure online)

Table 1 List of poses in the blind docking of DA targeting NF-κB p65/p50 (PDB: 1IKN), MMP-9 (PDB: 1GKC), and MMP-2 (PDB: 3AYU)

Poses	Binding affinities (kcal/mol)		
	NF-κB p65/p50	MMP-9	MMP-2
1	−8.4[a]	−8.2[a]	−8.0[a]
2	−8.1	−7.9[a]	−7.6
3	−8.0	−7.9[a]	−7.4[a]
4	−7.0	−7.6[a]	−7.3[a]
5	−6.9	−7.0[a]	−7.2
6	−6.5	−6.6[a]	−6.9
7	−5.8	−6.1[a]	−6.5
8	−5.3	−5.9[a]	−6.2
9	−5.2	−5.7[a]	−6.1
10	−4.4	−5.6[a]	−5.6
11		−5.3[a]	−5.2
12		−5.3[a]	−4.8
13		−5.2[a]	−4.7
14		−4.8[a]	−3.5
15			−3.0
16			−2.6

[a]Indicates that the ligand binds to the active region in protein

It was in agreement with the previous study to some extent (Hashimoto et al. 2011).

In conclusion, DA had the ability to penetrate into the active site of the key metastasis-related proteins such as MMP-2, MMP-9, and NF-κB p65/p50 and inhibit the biological action of proteins mainly through the hydrogen bonds.

Discussion

As the most frequently diagnosed cancer, lung cancer is the leading cause of death with a high incidence of metastatic pathology (Hsiao et al. 2018; Gong et al. 2018). Current primary therapeutic agents for lung cancer, including cisplatin, pemetrexed, and erlotinib, exhibited antitumor effects by impairing the structure and function of DNA, inhibiting cell proliferation, or suppressing epidermal growth factor receptor signal pathways (Tian et al. 2016; Rosell et al. 2002). Moreover, owing to their toxic side effects and drug resistance, these drugs were limitedly applied in clinical therapy. So it is urgent to find novel anti-metastasis candidates with low toxicity for lung cancers. As a natural steroidal saponin from *D. althaeoides* R. Knuth, its anti-proliferation and apoptotic-inducing effects were further verified, and its anti-metastasis activities on human lung cancer NCI-H460, NCI-H1299, NCI-H520 (NSCLC) and NCI-H446 (SCLC) cells were investigated in this study for the first time.

Tumor development and progression involve the cell transformation, deregulation of programmatic cell death, proliferation, invasion, angiogenesis, and metastasis (Si et al. 2016). It is of great importance in cancer therapy to interrupt cell proliferation. PCNA is a critical protein in regulating cell growth (Zhao et al. 2012). The present results demonstrated that DA significantly inhibited proliferation of four lung cancer cells by downregulation of PCNA.

Induction of apoptosis has been served as a promising approach for cancer therapy (Si et al. 2016). It occurs mainly through two pathways including the mitochondrial-mediated (intrinsic) apoptotic pathway and the cell-death-receptor-mediated (extrinsic) apoptotic pathway (Mi et al. 2016). Bcl-2 family members are closely involved in regulating the mitochondrial apoptotic pathway (Tseng et al. 2017). Consistent with the apoptosis effects of dioscin (Hsieh et al. 2013; Wei et al. 2013), DA triggered prominent apoptosis partially by activating caspase-9 and caspase-3, resulting in PARP cleavage in lung cancer cells. Moreover, DA treatment significantly upregulated the mRNA level of Bax and downregulated the mRNA level of bcl-2, thereby substantially increased Bax/bcl-2 ratio, indicating that the mitochondrial apoptotic pathway may be involved in DA-induced apoptosis in lung cancer cells (Chipuk et al. 2010). Besides, caspase-8 was involved in extrinsic apoptotic pathway activated by Fas and various apoptotic stimuli (Sui et al. 2014). A significant increase of caspase-8 was also detected in the DA-treated groups. All the above results were consistent with our previous study (Li et al. 2019). Taken together, the mitochondria-mediated pathway and activation of caspase-8 played important roles in the DA-induced apoptosis in human lung cancer cells.

Tumor metastasis is the leading cause of mortality associated with lung cancer. Numerous researches revealed that increased expression and activity of MMPs, particularly MMP-2 and MMP-9, promoted invasion in lung cancer cells (Gong et al. 2018; Ding et al. 2018). DA dramatically inhibited the invasive capacities NCI-H460, NCI-H1299, NCI-H520, and NCI-H446 human lung cancer cells based on the wound-healing assay. In addition, the expression of MMP-2 and MMP-9 were prominently decreased in a concentration-dependent manner after DA treatment in four lung cancer cells. The results were consistent with the anti-metastasis effects of dioscin (Si et al. 2016; Tao et al. 2017), suggesting that MMP-2 and MMP-9 at least partially participated in regulating human lung cancer cell migration.

NF-κB is a major sensor of cell stress closely connected with malignancy in many aspects. Promoting cell proliferation and migration as well suppression of apoptosis are its known roles in oncogenesis (Wu et al. 2018). It plays important role in the regulation of the production and activity of MMPs (Feng et al. 2014; Garg et al. 2010). Consistent with previous research, the mRNA levels of NF-κB, and the protein

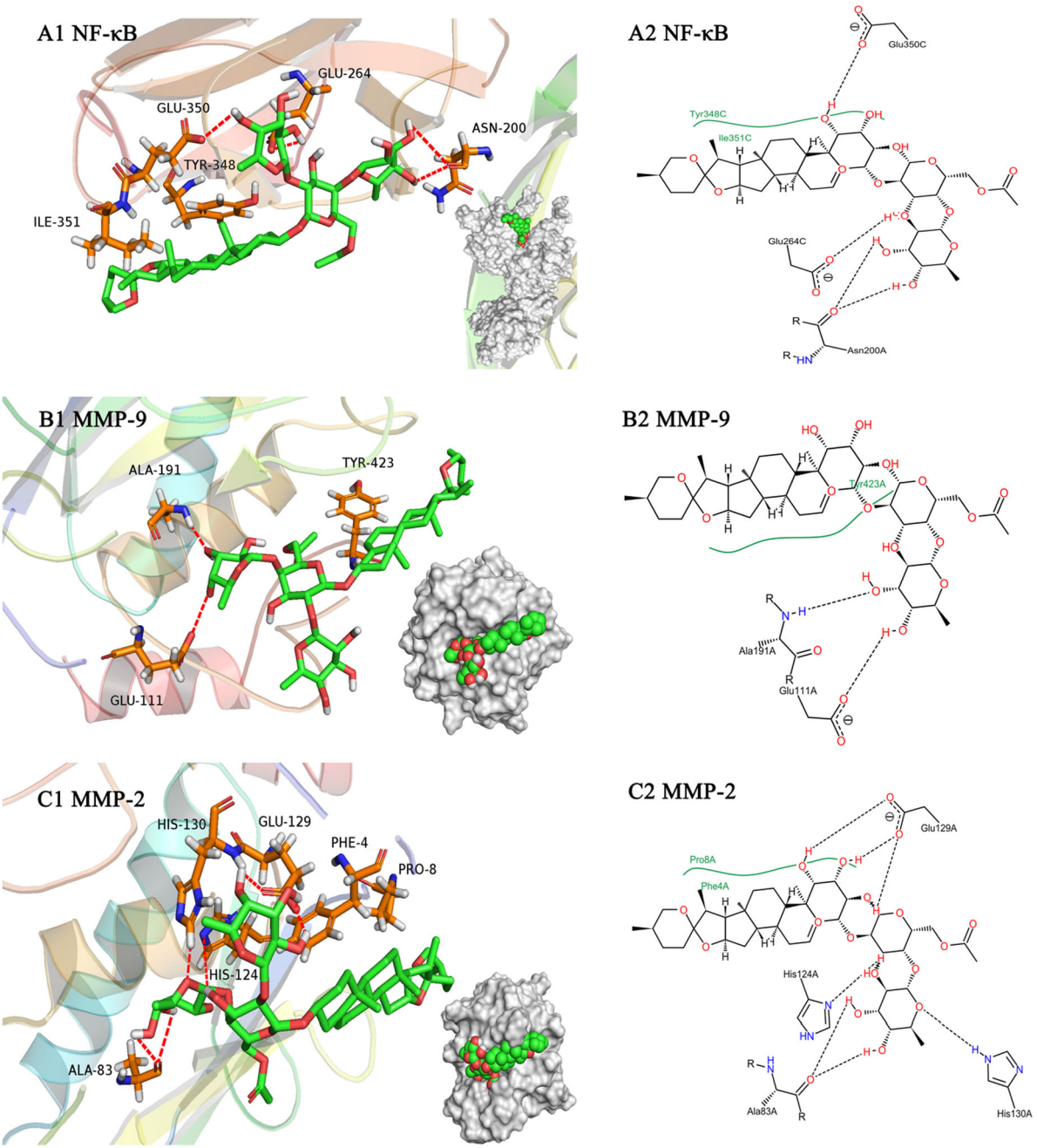

Fig. 7 3D and 2D intermolecular interactions of DA with **a** NF-κB p65/p50 (PDB: 1IKN), **b** MMP-9 (PDB: 1GKC), and **c** MMP-2 (PDB: 3AYU). The compound and important amino acids in the binding pockets are shown in the stick model, whereas proteins are depicted in the ribbon model (**a**1–**c**1). The interaction pattern is composed of hydrogen bonds (black) and hydrophobic contacts (green) (**a**2–**c**2). The figure was generated using PyMol and Poseview (color figure online)

expression of NF-κB p65 in the nucleus of four lung cancer cells, were all significantly downregulated by DA treatment. These results suggested that DA inhibited migration of human lung cancer cells via the downregulation of MMP-2/9 through NF-κB signaling suppression.

Moreover, docking study indicated that DA presented strong affinity with the key metastasis-related proteins such as MMP-2, MMP-9 and NF-κB p65/p50, and inhibited the biological action of proteins mainly through the hydrogen bonds.

In summary, we found that DA suppressed cell proliferation by downregulating PCNA, induced lung cancer apoptosis via activation of caspase-dependent apoptosis pathway, and inhibited lung cancer migration possibly by targeting MMP-2/9 through NF-κB signaling suppression (Fig. 9). The findings would provide a new theoretical basis

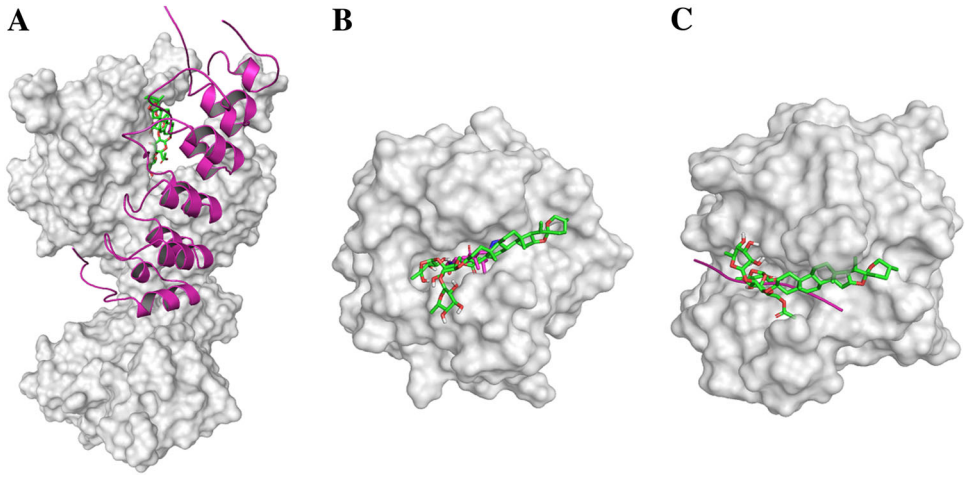

Fig. 8 Superimposition of ligand molecules within the **a** NF-κB p65/p50 (PDB: 1IKN), **b** MMP-9 (PDB: 1GKC), and **c** MMP-2 (PDB: 3AYU). Vin Violet is representativeed of the position of the inhibitor in the X-ray structure; green represents the position of DA obtained by docking (color figure online)

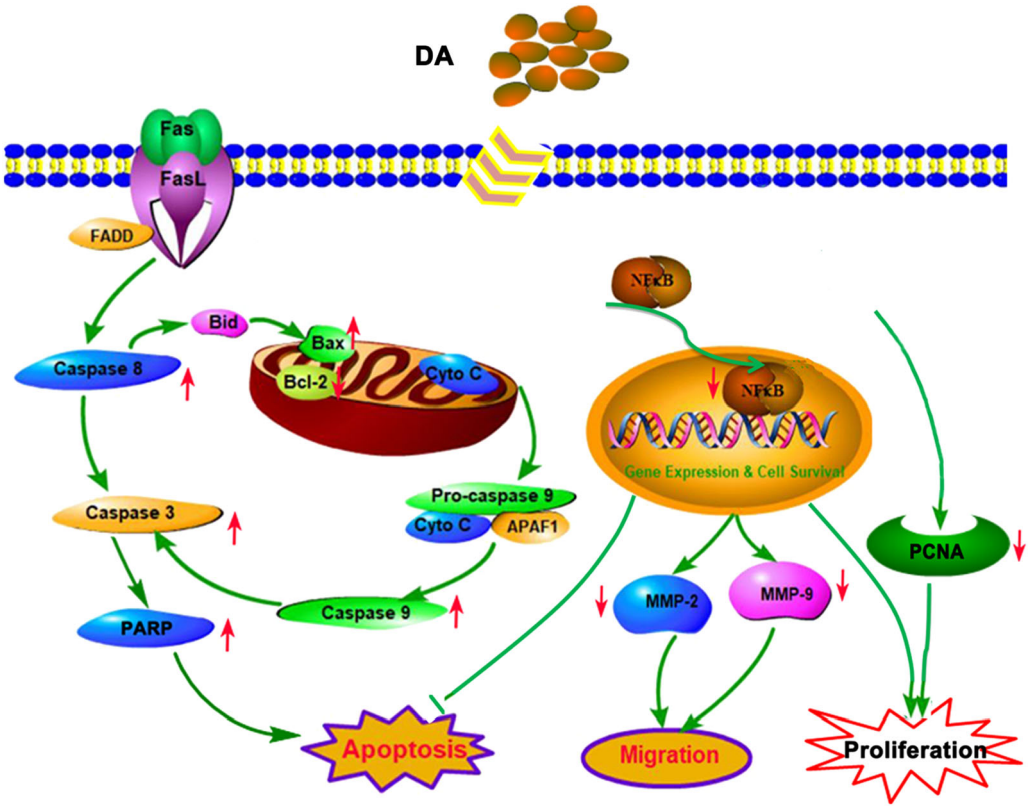

Fig. 9 Possible signaling pathways for antitumor effects of DA on human lung cancer cells

for the application of DA in molecular targeted therapy of lung malignancies.

Acknowledgements This work was financially supported by grant NOs. 81373904, 81673535, and 81173487 from the National Natural Science Foundation of China.

Compliance with ethical standards

Conflict of interest The authors declare that they have no conflict of interest.

References

Asghar MY, Kemppainen K, Lassila T, Tornquist K (2018) Sphingosine 1-phosphate attenuates MMP2 and MMP9 in human anaplastic thyroid cancer C643 cells: Importance of S1P2. PLoS ONE 13:e0196992

Chien MH, Ying TH, Hsieh YS, Chang YC, Yeh CM, Ko JL, Lee WS, Chang JH, Yang SF (2012) *Dioscorea nipponica* Makino inhibits migration and invasion of human oral cancer HSC-3 cells by transcriptional inhibition of matrix metalloproteinase-2 through modulation of CREB and AP-1 activity. Food Chem Toxicol 50:558–566

Chipuk JE, Moldoveanu T, Llambi F, Parsons MJ, Green DR (2010) The BCL-2 family reunion. Mol Cell 37:299–310

Ding C, Tang W, Fan X, Wang X, Wu H, Xu H, Xu W, Gao W, Wu G (2018) Overexpression of PEAK1 contributes to epithelial-mesenchymal transition and tumor metastasis in lung cancer through modulating ERK1/2 and JAK2 signaling. Cell Death Dis 9:802

El Gaafary M, Ezzat SM, El Sayed AM, Sabry OM, Hafner S, Lang S, Schmiech M, Syrovets T, Simmet T (2017) Acovenoside A induces mitotic catastrophe followed by apoptosis in non-small-cell lung cancer cells. J Nat Prod 80:3203–3210

Feng M, Wang Y, Chen K, Bian Z, Jinfang W, Gao Q (2014) IL-17A promotes the migration and invasiveness of cervical cancer cells by coordinately activating MMPs expression via the p38/NF-κB signal pathway. PLoS ONE 9:e108502

Garg P, Sarma D, Jeppsson S, Patel NR, Gewirtz AT, Merlin D, Sitaraman SV (2010) Matrix metalloproteinase-9 functions as a tumor suppressor in colitis-associated cancer. Cancer Res 70:792–801

Gong WJ, Liu JY, Yin JY, Cui JJ, Xiao D, Zhuo W, Luo C, Liu RJ, Li X, Zhang W, Zhou HH, Liu ZQ (2018) Resistin facilitates metastasis of lung adenocarcinoma through the TLR4/Src/EGFR/PI3K/NF-κB pathway. Cancer Sci 109:2391–2400

Hashimoto H, Takeuchi T, Komatsu K, Miyazaki K, Sato M, Higashi S (2011) Structural basis for matrix metalloproteinase-2 (MMP-2)-selective inhibitory action of β-amyloid precursor protein-derived inhibitor. J Biol Chem 286(38):33236–33243

Hsiao YT, Fan MJ, Huang AC, Lien JC, Lin JJ, Chen JC, Hsia TC, Wu RS, Chung JG (2018) Deguelin impairs cell adhesion, migration and invasion of human lung cancer cells through the NF-κB signaling pathways. Am J Chin Med 46:209–229

Hsieh MJ, Tsai TL, Hsieh YS, Wang CJ, Chiou HL (2013) Dioscin-induced autophagy mitigates cell apoptosis through modulation of PI3K/Akt and ERK and JNK signaling pathways in human lung cancer cell lines. Arch Toxicol 87:1927–1937

Huxford T, Huang DB, Malek S, Ghosh G (1998) The crystal structure of the IκBα/NF-κB complex reveals mechanisms of NF-κB inactivation. Cell 95:759–770

Jung O, Lee J, Lee YJ, Yun JM, Son YJ, Cho JY, Ryou C, Lee SY (2016) Timosaponin AIII inhibits migration and invasion of A549 human non-small-cell lung cancer cells via attenuations of MMP-2 and MMP-9 by inhibitions of ERK1/2, Src/FAK and β-catenin signaling pathways. Bioorg Med Chem Lett 26:3963–3967

Kim YJ, Jeon Y, Kim T, Lim WC, Ham J, Park YN, Kim TJ, Ko H (2017) Combined treatment with zingerone and its novel derivative synergistically inhibits TGF-β1 induced epithelial-mesenchymal transition, migration and invasion of human hepatocellular carcinoma cells. Bioorg Med Chem Lett 27:1081–1088

Li W, Yu X, Ma X, Xie L, Xia Z, Liu L, Yu X, Wang J, Zhou H, Zhou X, Yang Y, Liu H (2018a) Deguelin attenuates non-small cell lung cancer cell metastasis through inhibiting the CtsZ/FAK signaling pathway. Cell Signal 50:131–141

Li XJ, Qu Z, Jing SS, Li X, Zhao CC, Man SL, Wang Y, Gao WY (2019) Dioscin-6′-O-acetate inhibits lung cancer cell proliferation via inducing cell cycle arrest and caspase-dependent apoptosis Phytomedicine 53:124–133

Li XJ, Jing SS, Man SL, Li X, Zhao CC, Wang Y, Gao WY (2016) A new acetylated spirostanol saponin and other constituents from the rhizomes of *Dioscorea althaeoides* R. Knuth (Dioscoreaceae) Biochem Syst Ecol 65:17–22

Lim WC, Kim H, Kim YJ, Choi KC, Lee IH, Lee KH, Kim MK, Ko H (2017) Dioscin suppresses TGF-β1-induced epithelial-mesenchymal transition and suppresses A549 lung cancer migration and invasion. Bioorg Med Chem Lett 27:3342–3348

Liu Z, Zheng Q, Chen W, Wu M, Pan G, Yang K, Li X, Man S, Teng Y, Yu P, Gao W (2017) Chemosensitizing effect of Paris Saponin I on Camptothecin and 10-hydroxycamptothecin in lung cancer cells via p38 MAPK, ERK, and Akt signaling pathways. Eur J Med Chem 125:760–769

Lupinacci S, Perri A, Toteda G, Vizza D, Puoci F, Parisi OI, Giordano F, Lofaro D, La Russa A, Bonofiglio M, Bonofiglio R (2018) Olive leaf extract counteracts epithelial to mesenchymal transition process induced by peritoneal dialysis, through the inhibition of TGFβ1 signaling. Cell Biol Toxicol. https://doi.org/10.1007/s10565-018-9438-9

Mi Y, Xiao C, Du Q, Wu W, Qi G, Liu X (2016) Momordin Ic couples apoptosis with autophagy in human hepatoblastoma cancer cells by reactive oxygen species (ROS)-mediated PI3K/Akt and MAPK signaling pathways. Free Radic Biol Med 90:230–242

Rosell R, Lord RV, Taron M, Reguart N (2002) DNA repair and cisplatin resistance in non-small-cell lung cancer. Lung Cancer 3:217–227

Rowsell S, Hawtin P, Minshull CA, Jepson H, Brockbank SMV, Barratt DG, Slater AM, McPheat WL, Waterson D, Henney AM, Pauptit RA (2002) Crystal structure of MMP9 in complex with a reverse hydroxamate inhibitor. J Mol Biol 319:173–181

Si L, Zheng L, Xu L, Yin L, Han X, Qi Y, Xu Y, Wang C, Peng J (2016) Dioscin suppresses human laryngeal cancer cells growth via induction of cell-cycle arrest and MAPK-mediated mitochondrial-derived apoptosis and inhibition of tumor invasion. Eur J Pharmacol 774:105–117

Siegel RL, Miller KD, Jemal A (2016) Cancer statistics, 2016. CA Cancer J Clin 66:7–30

Siegel RL, Miller KD, Jemal A (2017) Cancer statistics, 2017. CA Cancer J Clin 67:7–30

Sui X, Kong N, Ye L, Han W, Zhou J, Zhang Q, He C, Pan H (2014) p38 and JNK MAPK pathways control the balance of apoptosis and autophagy in response to chemotherapeutic agents. Cancer Lett 344:174–179

Tao X, Xu L, Yin L, Han X, Qi Y, Xu Y, Song S, Zhao Y, Peng J (2017) Dioscin induces prostate cancer cell apoptosis through activation of estrogen receptor-β. Cell Death Dis 8:e2989

Tian L, Shen D, Li X, Shan X, Wang X, Yan Q, Liu J (2016) Ginsenoside Rg3 inhibits epithelial-mesenchymal transition (EMT) and invasion of lung cancer by down-regulating FUT4. Oncotarget 7:1619–1632

Trott O, Olson AJ (2010) AutoDock Vina: improving the speed and accuracy of docking with a new scoring function, efficient optimization, and multithreading. J Comput Chem 31:455–461

Tseng SC, Shen TS, Wu CC, Chang IL, Chen HY, Hsieh CP, Cheng CH, Chen CL (2017) Methyl protodioscin induces apoptosis in human osteosarcoma cells by caspase-dependent and MAPK signaling pathways. J Agric Food Chem 65:2670–2676

Wang S, Yan Y, Cheng Z, Hu Y, Liu T (2018) Sotetsuflavone suppresses invasion and metastasis in non-small-cell lung cancer A549 cells by reversing EMT via the TNF-α/NF-κB and PI3K/AKT signaling pathway. Cell Death Discov 4:26

Wei Y, Xu Y, Han X, Qi Y, Xu L, Xu Y, Yin L, Sun H, Liu K, Peng J (2013) Anti-cancer effects of dioscin on three kinds of human lung cancer cell lines through inducing DNA damage and activating mitochondrial signal pathway. Food Chem Toxicol 59:118–128

Wu DM, Han XR, Wen X, Wang S, Wang YJ, Shen M, Fan SH, Zhuang J, Zhang ZF, Shan Q, Li MQ, Hu B, Sun CH, Lu J, Zheng YL (2018) Long non-coding RNA LINC01260 inhibits the proliferation, migration and invasion of spinal cord glioma cells by targeting CARD11 via the NF-κB signaling pathway. Cell Physiol Biochem 48:1563–1578

Zhao H, Ho PC, Lo YH, Espejo A, Bedford MT, Hung MC, Wang SC (2012) Interaction of proliferation cell nuclear antigen (PCNA) with c-Abl in cell proliferation and response to DNA damages in breast cancer. PLoS ONE 7:e29416